Synthesis and Characterization of the Divalent Samarium Zintl-phases $SmMg_2Bi_2$ and $SmMg_2Sb_2$

D. Ramirez[a,b,*] , A. Gallagher[a], R. Baumbach[a], T. Siegrist[a,b]

[a] The National High Magnetic Field Laboratory, Condensed Matter Science Department, 1800 E. Paul Dirac Drive, Tallahassee, FL, 32310

[b] Florida State University, Department of Material Science and Engineering, 2005 Levy Ave., Tallahassee, FL 32310

[c] Florida Agricultural and Mechanical University-Florida State University College of Engineering, Department of Chemical and Biomedical Engineering, 2525 Pottsdamer St., Tallahassee, FL 32310

*Phone: (561)358-8324; Fax: (850) 644-5038; Email: ramirez@magnet.fsu.edu

KEYWORDS: Zintl-phase, Thermoelectric materials, X-ray diffraction, Van Vleck paramagnetism, Flux Synthesis

Abstract: Single crystals of $LnMg_2Bi_2$ (Ln = Yb, Eu, Sm) and $SmMg_2Sb_2$ were synthesized using Mg-Bi metal and Mg-Sb metal fluxes, respectively. The crystal structures are of the $CaAl_2Si_2$ type with space group $P\bar{3}m1$ (#164, Z = 1): $SmMg_2Bi_2$ (a = 4.7745(1)Å, c = 7.8490(2)Å), $EuMg_2Bi_2$ (a = 4.7702(1)Å, c = 7.8457(2) Å), $YbMg_2Bi_2$ (a = 4.7317(2)Å, c = 7.6524(3) Å), and $SmMg_2Sb_2$ (a = 4.6861(1) Å, c = 7.7192(2) Å). Heat capacity, electrical transport, and magnetization of all bismuth containing phases were measured. The materials behave as "poor metals" with resistivity between 2 and 10 mΩcm. Temperature independent Van Vleck paramagnetism is observed in $SmMg_2Bi_2$ indicative of divalent samarium (Sm^{2+}) ions.

Introduction

Zintl phases are a class of materials with a variety of properties, more specifically rare-earth Zintl-phases can provide an interesting mixture of magnetic and electronic properties. The classical definition of a Zintl phase is understood as a charge compensated material consisting of alkali or alkaline earth metals with p-block elements of groups 13 through 15. Exploration of the available elemental constituents and stoichiometry of these materials is an ongoing endeavor which employs various synthetic techniques.[1,2] One such class of materials is the $CaAl_2Si_2$ structure type (also referred to as the Ce_2O_2S type) which is a layered crystalline structure accommodating various elements. The structure and properties of these materials can be understood by the Zintl concept, with $Al_2Si_2^{2-}$ layers separated by Ca^{2+} monolayers (Figure 1a.).[3] Site preferences of the $Al_2Si_2^{2-}$ layer depend on the relative electronegativity of the elements[4], while the Ca^{2+} layer charge balances the materials[5-7].

The $CaAl_2Si_2$ structure type has been shown to accommodate a class of materials which can be developed for their thermoelectric properties; specifically the AMg_2Pn_2, AZn_2Pn_2, and ACd_2Pn_2 series of compounds where A = Ca, Sr, Eu, Yb; and Pn = pnictides: P, As, Sb, Bi. Thermoelectric figures of merit (zT) are given for $YbCd_{2-x}Zn_xSb_2$ zT = 1.2 at 700K,[8] $EuZn_2Sb_2$ zT = 0.9 at 700K,[9] and $YbMg_2Bi_2$ zT = 0.4 at 600K.[7] The tunability of these materials[10] is exemplified by the $YbCd_{2-x}Zn_xSb_2$ system, where the substitution of Zn for Cd is isoelectronic, but is found to optimize the electrical and thermal conductivity at x = 0.4.[8] Similar tunability is demonstrated in the $Yb_{1-x}Ca_xCd_2Sb_2$ system instead substituting on the cation layer.[11]

In the case of AMg_2Pn_2 and AZn_2Pn_2, the A-site of these materials have been shown to exclusively contain divalent ions,[3] which limits rare-earth ions to Sm, Eu, and Yb. However no samarium containing compounds have been reported to date. The study of materials containing divalent rare-earths has been mainly limited to europium and ytterbium, but should be also considered for samarium containing compounds. Here we describe the synthesis and characterization of the two new phases, $SmMg_2Bi_2$ and $SmMg_2Sb_2$. We present structural, magnetic, thermal, and electrical properties of AMg_2Bi_2 (A = Sm, Eu, Yb) single crystals and compare the results with previous investigations.

Experimental

Synthesis

Single crystals of $LnMg_2Bi_2$ (Ln = Yb, Eu, Sm) were grown and isolated from a molten Mg-Bi flux. The starting materials were elemental magnesium (Alfa-Aeser, 99.98%), elemental bismuth (Gallard-Schlesinger, 6N), and elemental rare-earth (Yb, Eu, Sm) metal (Aldrich 99.9%) in the molar ratio of 25:5:1 for Mg:Bi:Ln. $SmMg_2Sb_2$ crystals were grown from a corresponding Mg-Sb flux with elemental samarium also in a 25:5:1 molar ratio. The starting materials were loaded under ~1 atm Ar atmosphere into stainless steel crucibles that were subsequently welded shut and sealed in quartz ampoules under vacuum. The sealed ampoules were heated to 1000 °C

in 10 hours, held for 20 hours, and subsequently cooled to 700 °C over a period of 150 hours. At 700 °C the ampoules were removed from the furnace and centrifuged to separate the flux from the crystals.

The choice of molar ratios and heating profile is informed by the binary Mg-Bi phase diagram,[12] where the -Mg_3Bi_2 phase ($Im\bar{3}m$) region is avoided and the -Mg_3Bi_2 phase ($P\bar{3}m1$) region is targeted as the -phase is of $CaAl_2Si_2$-type. Previous synthesis methods of $LnMg_2Bi_2$ utilized Bi-rich fluxes (Mg:Bi ratio 4:6) and cooling to 650°C,[13] whereas the flux described in this work is magnesium rich, producing the largest crystals when cooling to 700°C. The flux is never slow-cooled into the liquid-solid two phase region, suggesting that the $LnMg_2Bi_2$ phases must have a higher stability than the corresponding $Mg(Mg_2Bi_2)$ phases. $SmMg_2Bi_2$ was only observed in fluxes with molar ratios of Mg:Bi:Sm of 25:5:1. The crystals are chemically stable, but show a decrease in luster after 48 hours in ambient conditions.

Phase Identification

EDS analysis using a JEOL 5900 scanning electron microscope confirmed the stoichiometry of $LnMg_2Bi_2$ having a molar Ln:Mg:Bi ratio of 1:2:2 to within 5 at.% (XRF2007 Software). The crystals were structurally characterized by single crystal x-ray diffraction using an Oxford-Diffraction Xcalibur2 CCD system with graphite monochromated MoK radiation. The as-grown crystals were transferred from the glovebox under Paratone-N oil and cleaved in the oil. Shards of appropriate size were selected, mounted in cryo-loops, and aligned in a cold nitrogen stream for data collections at 200 K. Reflections were recorded, indexed and corrected for absorption using the Oxford-Diffraction CrysAlis software making sure that reflections up to 100° in 2 were obtained.[14] Subsequent structure refinement was carried out using CRYSTALS[15]. Information regarding the data collection and results of the structural refinements are summarized in Tables 1, 2, and 3. The CIFs were deposited with ICSD (ICSD# 428792-428795).[16]

Magnetic, Electronic, and Physical Property Measurements

Temperature dependent magnetic susceptibility (χ=M/H) measurements were carried out using a Quantum Design MPMS SQUID system in the range of 2-300 K and at a field of 0.1 to 0.5 T. The single crystals were fixed with cotton wool inside a gel capsule and attached to a brass rod using an open ended plastic straw. A Quantum Design PPMS system was used to measure the zero-field heat capacity (C) in a temperature range of 0.4-20 K. The crystals were embedded in Apiezon N-grease; an addendum of the N-grease was taken prior to the experiment. Electrical resistivity (ρ) was measured using Van der Pauw 4-point contact geometry in the temperature range 1.8 K to 300 K using the same PPMS system. Gold leads were attached to single crystals using silver paste solvated in 2-butoxy-ethylacetate.

Results and Discussions

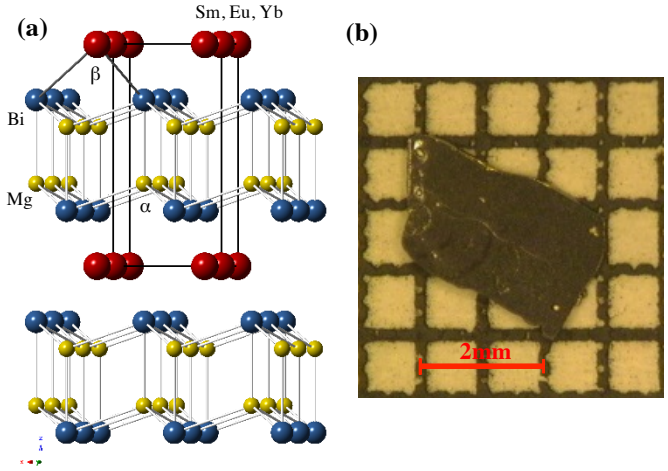

Figure 1. (a) Crystal structure with unit cell outlined of $LnMg_2Bi_2$ compounds. (b) Image of as grown $SmMg_2Bi_2$ crystal placed on a millimeter grid, the flat face is the (001) plane.

Structural Properties

The single crystals are metallic in appearance with a silver luster and plate-like morphology (Figure 1b). The large flat face is determined to be the ab-plane. The phases $LnMg_2Bi_2$ crystallize in the $CaAl_2Si_2$ structure type (trigonal, No. 164, $P\bar{3}m1$); results of the structure refinements are given in Table 1, atomic and thermal parameters in Table 2, and selected bond angles and distances in Table 3. The unit cell parameters of $SmMg_2Bi_2$ (a = 4.7745(1)Å, c = 7.8490(2) Å) and $EuMg_2Bi_2$ (a = 4.7702(1)Å, c = 7.8457(2)Å) are similar, with $SmMg_2Bi_2$ having slightly larger unit cell parameters in all directions, as expected from ionic radii considerations (Sm^{2+} 1.36Å compared to Eu^{2+} 1.31Å). For comparison, the ionic radius of Yb^{2+} is 1.16Å[17] resulting in smaller unit cell parameters for $YbMg_2Bi_2$ (a = 4.7317(2)Å c = 7.6524(3)Å) as observed. The similarity in ionic radii of Eu^{2+} and Sm^{2+} provides these analogs with similar structural properties and potentially mixed phases should be possible.[13] Our structural data agrees well with the data previously reported for the known compounds.

Table 1: Single crystal diffraction data and collection parameters for $LnMg_2Bi_2$, and $SmMg_2Sb_2$ collected at 200K

Space group: $P\bar{3}m1$ (#164) Z = 1	Parent Structure: $CaAl_2Si_2$			
Formula	$SmMg_2Sb_2$	$SmMg_2Bi_2$	$EuMg_2Bi_2$	$YbMg_2Bi_2$
ICSD#	428793	428792	428795	428794

a (Å)	4.6861 (1)	4.7745 (1)	4.7702 (1)	4.7317 (2)
c (Å)	7.7192 (2)	7.8490 (2)	7.8457 (2)	7.6524 (3)
vol ($Å^3$)	146.800 (6)	154.954 (7)	154.611 (6)	148.375 (10)
calc. density (g/cm^3)	5.005	6.611	6.643	7.158
Data collection range	5.02 < □ < 54.04	4.93 < □ < 53.92	4.94 < □ < 66.46	4.97 < □ < 54.01
Reflections	4660	4899	7102	4652
Independent refl.	742	769	1104	745
Parameters refined	10	9	9	10
R_1, wR_2 (all data)	0.0362, 0.0409	0.0447, 0.0529	0.0597, 0.0641	0.0381, 0.0447
Goodness-of-fit	0.9782	1.0651	1.0914	1.0890

Table 2: Refined structural parameters

		atomic coordinates			$U_{11} = U_{22}$	U_{33}	U_{eq}
	atom	x	y	z	$Å^2$	$Å^2$	$Å^2$
$SmMg_2Sb_2$	Sm	0	0	0	0.00889(8)	0.00829(10)	0.0087
	Mg	1/3	2/3	0.6304(2)	0.0105(4)	0.0098(6)	0.0103
	Sb	1/3	2/3	0.25380(3)	0.00748(7)	0.00765(9)	0.0075
$SmMg_2Bi_2$	Sm	0	0	0	0.01208(11)	0.01183(16)	0.0120
	Mg	1/3	2/3	0.6279(4)	0.0142(7)	0.0129(10)	0.0138
	Bi	1/3	2/3	0.25032(3)	0.01033(8)	0.01103(10)	0.0106
$EuMg_2Bi_2$	Eu	0	0	0	0.01391(10)	0.01517(13)	0.0143
	Mg	1/3	2/3	0.6283(5)	0.0159(6)	0.0174(9)	0.0164
	Bi	1/3	2/3	0.25009(3)	0.01216(7)	0.01434(8)	0.0129
$YbMg_2Bi_2$	Yb	0	0	0	0.01846(13)	0.01643(17)	0.0092
	Mg	1/3	2/3	0.6313(5)	0.0174(8)	0.0164(11)	0.0087
	Bi	1/3	2/3	0.24123(4)	0.01466(8)	0.01446(11)	0.0073

Table 3: Bond distances and angles for $LnMg_2Bi_2$ and $SmMg_2Sb_2$

	bond distances (Å)		bond angles (deg)	
SmMg2Sb2	Sm – Sb (1)	3.3404(2)	Sb – Sm – Sb (□)	89.080(5)
	Mg – Sb (2)	2.8494(6)	Sb – Mg – Sb (□)	110.583(3)
	Sm – Sm (3)	4.6861 (1)		
SmMg2Bi2	Sm – Bi (1)	3.3851(1)	Bi – Sm – Bi (□)	89.699(5)
	Mg – Bi (2)	2.918(1)	Bi – Mg – Bi (□)	109.807(6)
	Sm – Sm (3)	4.7745 (1)		
EuMg2Bi2	Eu – Bi (1)	3.382(1)	Bi – Eu – Bi (□)	89.714(4)
	Mg – Bi (2)	2.915(1)	Bi – Mg – Bi (□)	109.825(7)
	Eu – Eu (3)	4.7702 (1)		
YbMg2Bi2	Yb – Bi (1)	3.2966(2)	Bi – Yb – Bi (□)	91.709(7)
	Mg – Bi (2)	2.899(2)	Bi – Mg – Bi (□)	109.285(8)
	Yb – Yb (3)	4.7317 (2)		

Physical properties

$SmMg_2Sb_2$

Single crystals of $SmMg_2Sb_2$ were sufficiently large for x-ray diffraction studies; however the electronic property studies of the material were challenging and were not performed. The following results are for $LnMg_2Bi_2$ (Ln = Sm, Eu, and Yb)

Magnetism

The magnetic susceptibility data $\chi = M/H$ (H = 0.5T) versus temperature for single crystal $SmMg_2Bi_2$ is shown in Fig. 2.

Van Vleck paramagnetic behavior is observed with a susceptibility plateau between 10K and 100K and a Curie tail developing below 10K. The plateau region is typical of ions with electron configuration $4f^6$ and is seen in compounds containing Eu^{3+} ions,[18] but is also notable in Sm^{2+} systems such as the samarium monochalcogenides[19] or SmB_6.[20] The Curie tail is likely attributed to magnetic impurities within the sample such as Sm^{3+} cations or contamination from the stainless steel crucibles.

The magnetic susceptibility temperature dependence was modeled for $SmMg_2Bi_2$ using a Russel-Saunders coupling scheme for the spin-orbit interaction, where □L·S represents

the separation in ^7F_J multiplets in divalent Sm^{2+}. The following Van Vleck model is used to fit the data:

$$\chi_{Sm^{2+}} = N\frac{\sum_0^6\left[\frac{g^2\mu_B^2J(J+1)}{3k_BT}+\alpha_J\right](2J+1)e^{-E_J/k_BT}}{\sum_0^6(2J+1)e^{-E_J/k_BT}} \quad (1)$$

The expression is summed over the various multiplet states (J = 0 to 6) with $E_J = J\lambda + E_{j-1}$.[18] The coupling constant is the energy difference between the ground state and first excited state, and J is the total angular momentum for Sm^{2+}. The α_J term is a second order Zeeman term which represents the mixing of mutliplet states for J and J±1.[21] This is defined as:

$$\alpha_J = \frac{\mu_B^2}{6(2J+1)}\left[\frac{F_{J+1}}{E_{J+1}-E_J} - \frac{F_J}{E_J - E_{J-1}}\right]$$

with

$$F_J = \frac{[(L+S+1)^2 - J^2][J^2 - (S-L)^2]}{J}$$

The addition of a modified Curie law is used to model the susceptibility due to impurities. In the case of the presence of Sm^{3+}, the following simple expression can be used:

$$\chi_{Sm^{3+}} = \frac{C}{T} + \chi_0 \quad (2)$$

Here, χ_0 is attributed to coupling between the ground J=5/2 state and the J =7/2 state allowed due to the small energy difference between the multiplets.[21-23] The total magnetism is therefore:

$$\chi_{Total} = \chi_{Sm^{2+}} + \chi_{Sm^{3+}} \quad (3)$$

The susceptibility data is shown in figure 2 with orientation H⊥c and H‖c under a field of 0.5T. Magnetic anisotropy is seen, with a slightly larger susceptibility resulting from H applied ‖ c. The results of the fit (eq. 3) are presented in table 4. The coupling constants λ for H‖c and H⊥c are 409K and 450K respectively, which are in agreement with Van Vleck's theoretical work of 418K for free ions with the configuration $[Xe]4f^6$.[21] In figure 2 the solid lines are the susceptibility fits (eq. 3), the Sm^{2+} contribution (eq. 1) is plotted as a dashed line, and the impurity susceptibility (eq. 2) is plotted as the dotted line below the break. Sm^{2+} ions dominate the behavior of the magnetic susceptibility providing more than 95% of the overall moment. The most notable contribution from the impurities appear below 10K. If we attribute the magnetic impurities to Sm^{3+} ions, the concentration can be estimated from the fit for the Curie term. Using the effective moment for Sm^{3+} (μ_{eff} = 0.85μ_B)[21] with the obtained Curie constant C, the amount of Sm^{3+} impurities is found to be of the order of 0.7%. If the experimental moment for Sm^{3+} free ions (μ_{eff} = 1.54μ_B)[21] is used, a lower concentration of the order of 0.2% is found.

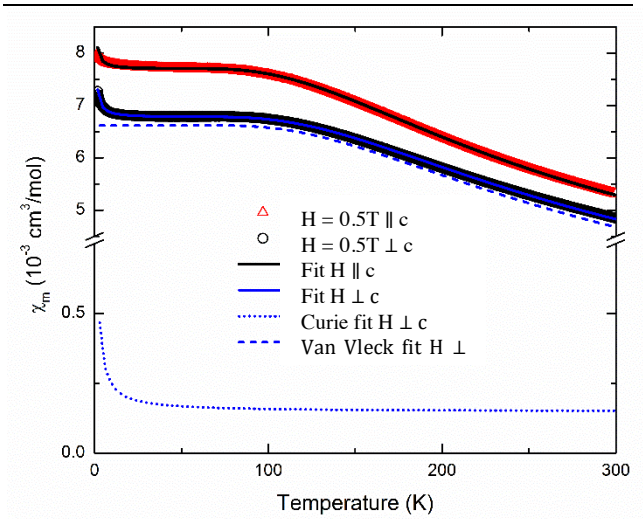

Figure 2: vs T for $SmMg_2Bi_2$ single crystal at a field of 0.5T. The solid curves are the total fits using equation (3), the Curie fit equation (2) is represented by the dotted line, and the Van Vleck fit equation (1) is represented by the dashed line. The parameters resulting from the fit are given in table 4.

Table 4: Fit parameters for $SmMg_2Bi_2$ magnetic susceptibility

	H⊥c	H‖c
(K)	450	409
C (cm3/mol·K)	7.32x10-4	5.57x10-4
0 (cm3/mol)	1.21x10-4	3.65x10-4
Sm3+ (eff = 0.85B)	0.81%	0.62%
Sm3+ (eff = 1.54B)	0.25%	0.18%

Single crystals of $EuMg_2Bi_2$ show Curie-Weiss behavior followed by antiferromagnetic ordering with a T_N around 7K (Fig. 3). The larger susceptibility of the samples with c-axis orientation ⊥ to the field indicates the magnetic moments are aligned along the c-axis. A Curie-Weiss fit to the paramagnetic region yields an effective moment of 7.98 μ_B per Eu atom, in agreement with expectations from Hund's rules. The Weiss temperature of -3.6K is in agreement with the ordering temperature, and previous work[13].

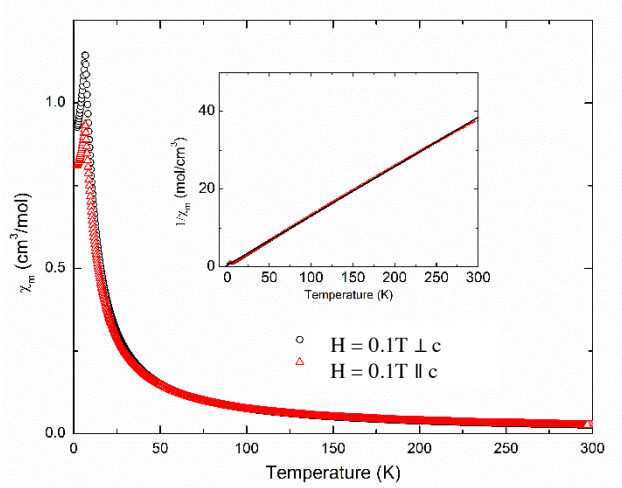

Figure 3: χ_m vs T for $EuMg_2Bi_2$ single crystal at a field of 0.1T. An antiferromagnetic transition is observed at 7K. The inset is a plot of χ_m^{-1} vs T with a linear fit yielding μ_{eff} = 7.98μ_B and a Weiss temperature of -3.6K

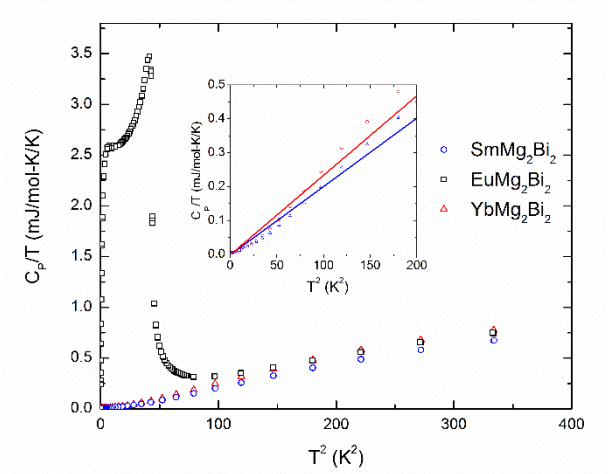

Figure 4: C_p/T versus T^2 for the measured compounds from 0.4 – 20K. The inset provides low temperature data for the non-magnetic compounds.

Heat capacity

Results from heat capacity for $LnMg_2Bi_2$ (Ln = Sm, Eu, Yb) are shown in Figure 4. The results for the non-magnetic compounds (Sm, Yb) are typical for semi-metal compounds. The inset in figure 4 illustrates the temperature dependence of the specific heat plotted as C_p/T vs T^2. This data is fitted to the relation

$$\frac{C_p}{T} = \gamma + \beta T^2$$

where γ denotes the Sommerfeld coefficient of the electronic contribution and β denotes the coefficient of the lattice contribution. The fit yields the values $\gamma \approx$ -0.0016(20) J/molK^2 for $SmMg_2Bi_2$ and $\gamma \approx$ -0.0013(20) J/molK^2 for $YbMg_2Bi_2$ with $\beta \approx$ 0.0020(20) J/molK^4 and $\beta \approx$ 0.0024(20) J/molK^4. The gamma term is essentially zero within measurement accuracy and therefore indicates an electron poor system with little electronic contribution to the heat capacity. A Debye integral fit of the nonmagnetic data provides Debye temperatures of Θ_D = 138K and 130K for $SmMg_2Bi_2$ and $YbMg_2Bi_2$, respectively. This result suggests that the lattice is quite soft, by comparison to typical ternary rare-earth intermetallics such as $TbCu_2Si_2$ which provides a Θ_D = 201K[24].

The antiferromagnetic ordering of $EuMg_2Bi_2$ at 7K is clearly observed in the heat capacity measurements. The entropy change for the magnetic transition is predicted to be 17.3 J/mol-K by $\Delta S = R\ln(2J+1)$ where J = 7/2 for Eu^{2+}.[25] Since the phonon contributions to heat capacity for both $EuMg_2Bi_2$ and $SmMg_2Bi_2$ should be similar due to similar structure parameters, $SmMg_2Bi_2$ is used as a nonmagnetic reference to find the entropy change of the antiferromagnetic phase transition, resulting in ΔS = 16.7 J/mol·K. However it can be observed from figure 4 that some residual entropy remains in the system below 7K possibly due to some remaining spin degrees of freedom. Similar antiferromagnetic behavior has been observed in other rare-earth containing compounds of various crystal structures.[26-28]

Electronic Transport

All phases measured behaved similarly showing semi-metallic behaviour. These materials are expected to be semiconductors as determined by electronic structure calculations[13]. Hall probe transport measurements previously used to determined the carriers to be p-type[5,13]. The carrier type was verified as p-type conductivity at room temperature using a nanovoltmeter and applying a temperature gradient to the single crystals. The results for $SmMg_2Bi_2$ are shown as the inset of figure 5. A positive change in voltage results from applying a heat to the negative terminal, and a negative change in voltage results from applying heat to the positive terminal indicitave of p-type carriers.[29] In $EuMg_2Bi_2$ the antiferromagnetic transition can be seen as a gradual increase in resistivity as the temperature decreases towards 7K, with an abrupt decrease in resistivity below 7K as expected from the magnetic ordering of the sample removing magnetic scattering of the carriers. The $SmMg_2Bi_2$ and $YbMg_2Bi_2$ samples behave similar in resistivity, with Yb having a slightly higher resistivity. RRR values were determined by taking ρ(300K)/ρ(10K); giving 2.04, 2.40, and 1.57 for $SmMg_2Bi_2$, $YbMg_2Bi_2$, and $EuMg_2Bi_2$ respectively.

All our samples show higher resistivity and larger RRR than previously reported. This follows the previous assertion suggesting the carrier concentration of these materials arise from impurities and defects[6,13]. The magnetic susceptibility data for $SmMg_2Bi_2$ suggests the presence of Sm^{3+} impurities of around 0.2-0.7% which can account for the p-type conductivity.

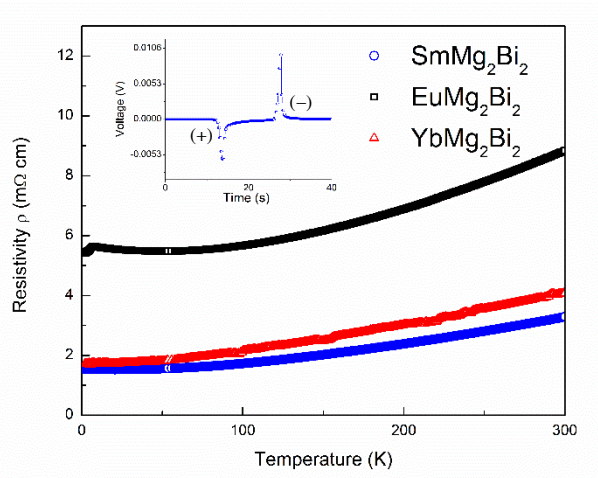

Figure 5: Resistivity of all Bi-containing compounds between 1.8K and 300K. The inset is the voltage through the sample with heat applied to the positive terminal (+) and to the negative terminal (-).

Conclusion

Divalent samarium in $SmMg_2Sb_2$ and $SmMg_2Bi_2$ is stabilized in mixed magnesium rich fluxes. Electronic transport studies show that the materials behave as poor metals suggesting conduction is the result of sample impurities. The magnetic behavior was successfully modeled using Van Vleck theory for ions having the $[Xe]4f^6$ electronic state, proving the presence of Sm^{2+}. The magnetism data was also used to estimate the existence of 0.2% to 0.7% Sm^{3+} ions in the system, which would contribute to the conductivity of the materials. The similarity between the structures for $SmMg_2Bi_2$ and $EuMg_2Bi_2$ allowed accurate calculation of the entropy of the antiferromagnetic transition of $EuMg_2Bi_2$.

Two new compounds $SmMg_2Bi_2$ and $SmMg_2Sb_2$ along with the previously discovered $YbMg_2Bi_2$ and $EuMg_2Bi_2$ analogs were synthesized as single crystals using Mg-rich Mg-Bi/Sb fluxes. Single crystals of $SmMg_2Sb_2$ were synthesized; however the mixed flux method did not provide crystals large enough for thorough characterization. The electronic properties of the Sb analogs would be expected to be similar to the Bi analogs. It is expected that $SmMg_2As_2$ and $SmMg_2P_2$ compounds should also be possible to obtain.[1] Ln_2O_3 starting materials were shown to produce the desired phases, albeit at lower yields than if pure lanthanide metals were used. This can be ascribed to the highly reducing nature of the Mg-rich flux with MgO as a byproduct upon reduction of Ln_2O_3 to Ln. The measured properties of the materials are consistent with the previously observed properties.

Acknowledgements

This research is supported by the US Department of Energy, Office of Basic Energy Sciences, Division of Materials Sciences under Award DE-SC0008832 (T.S., D.R. synthesis and structural characterization of samples). A portion of this work was performed at the National High Magnetic Field Laboratory, which is supported by National Science Foundation Cooperative Agreement No. DMR-1157490, the State of Florida, and the U.S. Department of Energy. We would also like to acknowledge Eden Steven, Tiglet Besara, and Jefferey Whalen for their productive input.

References

1. *Zintl Phases: Principles and Recent Developments*. **139,** (Springer Berlin Heidelberg, 2011).

2. Westbrook, J. & Fleischer, R. *Intermetallic Compounds: Vol. 3, Principles and Practice*. (John Wiley & Sons, Ltd., 2002).

3. Burdett, J. K. & Miller, G. J. Fragment formalism in main-group solids: applications to aluminum boride (AlB_2), calcium aluminum silicide ($CaAl_2Si_2$), barium-aluminum (BaAl4), and related materials. *Chem. Mater.* **2,** 12–26 (1990).

4. Zheng, C., Hoffmann, R., Nesper, R. & Von Schnering, H. G. Site preferences and bond length differences in $CaAl_2Si_2$-type Zintl compounds. *J. Am. Chem. Soc.* **108,** 1876–1884 (1986).

5. Imai, M., Abe, H. & Yamada, K. Electrical Properties of Single-Crystalline $CaAl_2Si_2$. *Inorg. Chem.* **43,** 5186–5188 (2004).

6. May, A. F. *et al.* Properties of single crystalline AZn_2Sb_2 (A=Ca,Eu,Yb). *J. Appl. Phys.* **111,** 033708 (2012).

7. May, A. F. *et al.* Thermoelectric transport properties of CaMg2Bi2, EuMg2Bi2, and YbMg2Bi2. *Phys. Rev. B* **85,** (2012).

8. Wang, X.-J. *et al.* Synthesis and high thermoelectric efficiency of Zintl phase $YbCd_{2-x}Zn_xSb_2$. *Appl. Phys. Lett.* **94,** 092106 (2009).

9. Zhang, H. *et al.* A new type of thermoelectric material, $EuZn_2Sb_2$. *J. Chem. Phys.* **129,** 164713 (2008).

10. Toberer, E. S., May, A. F. & Snyder, G. J. Zintl Chemistry for Designing High Efficiency Thermoelectric Materials. *Chem. Mater.* **22,** 624–634 (2009).

11. Cao, Q.-G. *et al.* Zintl phase $Yb_{1-x}CaxCd_2Sb_2$ with tunable thermoelectric properties induced by cation substitution. *J. Appl. Phys.* **107,** 053714 (2010).

12. Massalski, T. *Binary Alloy Phase Diagrams*. **1,** (ASM International, 1992).

13. May, A. F., McGuire, M. A., Singh, D. J., Custelcean, R. & Jellison, G. E. Structure and Properties of Single Crystalline $CaMg_2Bi_2$, $EuMg_2Bi_2$, and $YbMg_2Bi_2$. *Inorg. Chem.* **50,** 11127–11133 (2011).

14. Agilent Technologies, *CrysAlisPro*, Version 171.36. Agilent Technologies UK Ltd., Oxford, UK, 2012.

15. Betteridge, P. W., Carruthers, J. R., Cooper, R. I., Prout, K. & Watkin, D. J. CRYSTALS version 12: software for guided crystal structure analysis. *J. Appl. Crystallogr.* **36,** 1487–1487 (2003).

16. Bergerhoff, G. & Brown, I. D. *in Crystallographic Databases, F.H. Allen et al.* (International Union of Crystallography, 1987).

17. Gaft, M., Reisfeld, R. & Panczer, G. *Modern Luminescence Spectroscopy of Minerals and Materials*. (Springer Science & Business Media, 2005).

18. Takikawa, Y., Ebisu, S. & Nagata, S. Van Vleck paramagnetism of the trivalent Eu ions. *J. Phys. Chem. Solids* **71,** 1592–1598 (2010).

19. Bucher, E., Narayanamurti, V. & Jayaraman, A. Magnetism, Metal–Insulator Transition, and Optical Properties in Sm– and Some Other Divalent Rare–Earth Monochalcogenides. *J. Appl. Phys.* **42,** 1741–1745 (1971).

20. Nickerson, J. C. *et al.* Physical Properties of SmB_6. *Phys. Rev. B* **3,** 2030–2042 (1971).

21. Van Vleck, J. *The Theory of Electric and Magnetic Susceptibilities*. (Oxford University Press, 1932).

22. Pospíšil, J., Kratochvílová, M., Prokleška, J., Diviš, M. & Sechovský, V. Samarium magnetism studied on $SmPd_2Al_3$ single crystal. *Phys. Rev. B* **81,** 024413 (2010).

23. Vališka, M. *et al.* Influence of symmetry on Sm magnetism studied on $SmIr_2Si_2$ polymorphs. *J. Alloys Compd.* **574,** 459–466 (2013).

24. Szytu–a, A. *et al.* Specific heat studies of RCu_2Si_2 (R=Tb, Ho) and RCu_2Ge_2 (R=Gd, Tb) compounds. *Solid State Commun.* **152,** 155–159 (2012).

25. Smart, J. S. & Vleck, J. H. V. *Effective Field Theories of Magnetism*. (W.B. Saunders company, 1966).

26. Welter, R. & Halich, K. A magnetic study of the ThCr2Si2-type RPd2Ge2 (R=Pr, Nd) compounds. Magnetic structure of PrPd2Ge2 from powder neutron diffraction. *J. Phys. Chem. Solids* **67,** 862–867 (2006).

27. Tung, L. D., Franse, J. J. M., Buschow, K. H. J., Brommer, P. E. & Thuy, N. P. A study of magnetic coupling in GdT_2Si_2 compounds (T=transition metal). *J. Alloys Compd.* **260,** 35–43 (1997).

28. Bauer, E. D. *et al.* Investigation of ferromagnetic filled skutterudite compounds EuT_4Sb_{12} (T = Fe, Ru, Os). *J. Phys. Condens. Matter* **16,** 5095 (2004).

29. Steven, E. *et al.* Physical characterization of functionalized spider silk: electronic and sensing properties. *Sci. Technol. Adv. Mater.* **12,** 055002 (2011).